Plasmonic Polymer Tandem Solar Cell

Jun Yang,[†,⊥] Jingbi You,[†,⊥] Chun-Chao Chen,[†] Wan-Ching Hsu,[†] Hai-ren Tan,[‡] Xing Wang Zhang,[‡] Ziruo Hong,[§] and Yang Yang[†,*]

[†]Department of Materials Science and Engineering and California NanoSystems Institute, University of California Los Angeles, Los Angeles, California 90095, United States, [‡]Key Lab of Semiconductor Materials Science, Institute of Semiconductors, Chinese Academy of Science, Beijing, 100083, People's Republic of China, and [§]Graduate School of Science and Enginnering, Yamagata University, Yonezawa, Yamagata, 9928510, Japan. [⊥]These authors contributed equally to this work.

ABSTRACT We demonstrated plasmonic effects in an inverted tandem polymer solar cell configuration by blending Au nanoparticles (NPs) into the interconnecting layer (ICL) that connects two subcells. Experimental results showed this plasmonic enhanced ICL improves both the top and bottom subcells' efficiency simultaneously by enhancing optical absorption. The presence of Au NPs did not cause electrical characteristics to degrade within the tandem cell. As a result, a 20% improvement of power conversion efficiency has been attained by the light concentration of Au NPs *via* plasmonic near-field enhancement. The simulated near-field distribution and experimental Raman scattering investigation support our results of plasmonic induced enhancement in solar cell performance. Our finding shows a great potential of incorporating the plasmonic effect with conventional device structure in achieving highly efficient polymer solar cells.

KEYWORDS: polymer solar cell · tandem solar cell · plasmonic effect · gold nanoparticles · interconnecting layer

Polymer-based organic photovoltaic systems hold promise for a cost-effective, lightweight solar energy conversion platform, which could benefit from simple solution processing of the active layer.[1−3] At present, organic bulk heterojunction solar cells show power conversion efficiencies (PCE) up to 7%.[4,5] The quantum efficiency of organic solar cells is, however, still limited by the comparatively low carrier mobility.[6] A thinner active layer can lower the probability of charge recombination and increase the carrier drift velocity by having a higher electric field, thus enhancing the internal quantum efficiency. However, a minimum film thickness is always required to ensure sufficient photon absorption.[6,7] Therefore, how to increase the light absorption of a polymer film at a limited thickness of film still remains a challenge. Recently, metallic nanostructures have been introduced into thin inorganic semiconductor solar cells (*e.g.*, Si, GaAs solar cells) for highly efficient light harvesting by expected light-scattering behavior and a strong near-field by the plasmonic effect of metallic nanostructures.[8−13] More recently, the plasmonic effect is demonstrated in single bulk heterojunction polymer solar cells[14−16] and small molecule single and tandem solar cells[17,18] with an observable improvement in PCE, which is mainly ascribed to the light-concentrating effect caused by the plasmonic scattering or near-field enhancement.[19,20] Polymer tandem solar cells, a multilayer structure including several semiconductors with different band gaps, have spurred much interest due to their advantage in harvesting a wider range of the solar spectrum.[21,22] Therefore the plasmonic effect has the potential to be utilized in polymer tandem solar cells to help convert more light into solar energy, resulting in higher efficiency. Unfortunately, until now, a plasmonic enhanced polymer tandem solar cell has not yet been reported due to the difficulty in demonstrating metal nanostructures in the device structure. Poly(3,4-ethylenedioxythiophene) poly(styrenesulfonate) (PEDOT:PSS) as an important buffer layer for polymer solar cells is selected as an attractive candidate in incorporating metal nanoparticles (NPs) for achieving an effective plasmonic effect in polymer solar cells.[23] In our design by using a PEDOT:metal NP hybrid layer as an interconnecting layer (ICL) of tandem solar cell, the plasmonic effect is triggered in the middle of the ICL, which can potentially enhance the absorption of both top and bottom subcells simultaneously. In this study, Au NPs have been introduced into the PEDOT:PSS layer as an ICL for polymer tandem solar cells, and the results demonstrated 20% efficiency enhancement due to the effect of a Au NPs generated plasmonic near-field.

RESULTS AND DISCUSSION

To demonstrate the plasmonic effect in polymer tandem solar cells, subcells

* Address correspondence to yangy@ucla.edu.

Received for review March 21, 2011 and accepted July 12, 2011.

Published online 10.1021/nn202144b

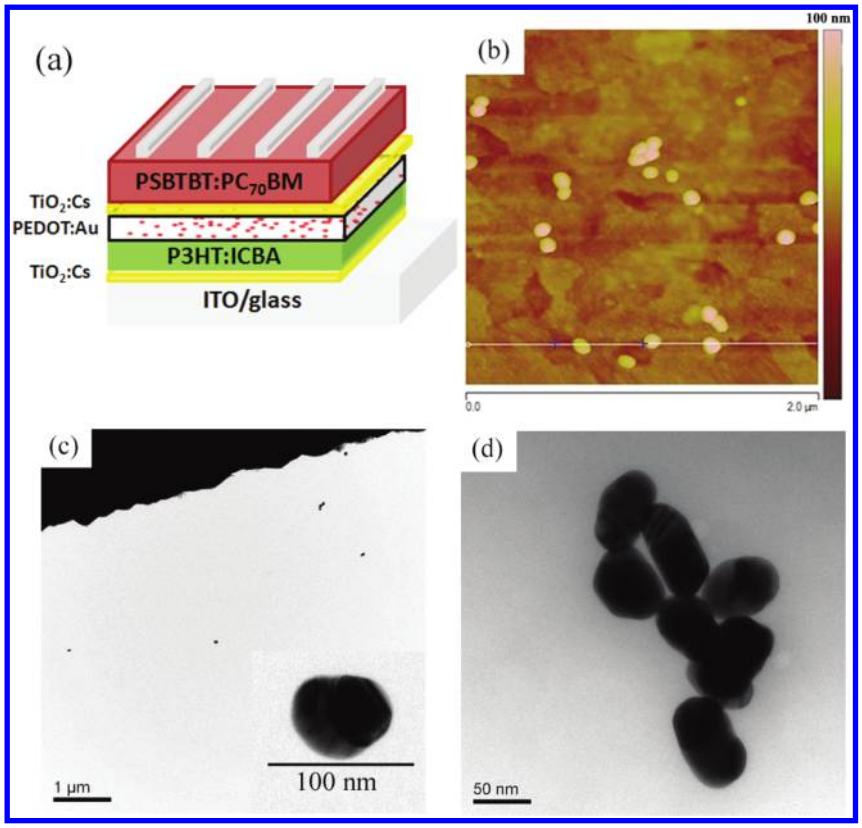

Figure 1. (a) Schematic of plasmonic polymer tandem solar cell, ITO/TiO_2:Cs/P3HT:$IC_{60}BA$/PEDOT:Au/TiO_2:Cs/PSBTBT:$PC_{70}BM$/MoO_3/Al, (b) AFM images of monolayer Au NPs adsorbed on ITO substrate, (c) TEM images of Au NPs, (inset) magnified TEM image of Au NPs, and (d) TEM image of PEDOT:Au.

including poly(3-hexylthiophene) (P3HT):indene-C_{60} bisadduct ($IC_{60}BA$) as a front cell[24] and poly[(4,4′-bis(2-ethylhexyl)dithieno[3,2-*b*:2′,3′-*d*]silole)-2,6-diyl-alt-(2,1,3-benzothiadiazole)-4,7-diyl] (PSBTBT):[6,6]-phenyl-C_{71}-butyric acid methyl ester ($PC_{70}BM$)[25] as the rear cell were adopted, and the structure of the plasmonic tandem solar cell is shown in Figure 1a. In this structure, the absorption profiles of P3HT and PSBTBT end at 650 and 850 nm, respectively (their absorption spectra will be shown later), which complementarily cover a broad band of absorption and satisfy the requirement of tandem solar cells. An ICL, consisting of PEDOT:PSS and TiO_2:Cs, is introduced as anode and cathode, respectively, to connect the front and rear cells in series.[26] To avoid layers of the front cell from being dissolved during the deposition of the rear cell, a robust and thick PEDOT:PSS (80 nm) layer was spun coated (or spray coated) on the top of the front cell, and the step profile of the PEDOT:PSS layer is shown in Figure S1.[26] To induce a localized surface plasmon within the device structure, the nanoparticles are placed close to the active layer in order to utilize its near-field strength as much as possible. In this case the similar size (about 70−80 nm) of the Au nanoparticles (NPs) was blended into the PEDOT:PSS solution and coated on top of the active layer. The atomic force microscopy (AFM) image of monolayer Au NPs adsorbed on the ITO surface is shown in Figure 1b. From the corresponding section line, it can be found that the height of Au NPs is estimated to be 70−80 nm, which is comparable to the thickness of the PEDOT:PSS layer. Therefore, it is anticipated that Au NPs are planted into the PEDOT:PSS matrix uniformly. To investigate the states of Au NPs in PEDOT, transmission electron microscopy (TEM) was used to characterize the topography of the PEDOT:Au film in comparison with the pure Au NPs film. The TEM images of pure Au NPs and PEDOT:Au blend are shown in Figure 1c and d, respectively. It can be seen from the magnified TEM image of Au NPs in the inset of Figure 1c that the Au NPs are isolated and well dispersed in solution, and the particle size is estimated to be about 72 nm accordingly. As shown in Figure 1d, it is also found that Au NPs aggregate within PEDOT; this will lead to the extension of the surface plasmon properties due to particle−particle interaction.[27,28] The film properties of PEDOT, such as absorption (transmittance), thickness, and electrical conductivity, have not been significantly changed with or without blending Au NPs (the results are shown in Figure S2 and Table S1). It is worth mentioning that the Au NPs with a plasmonic extinction peak have not been observed, inferring the low concentration of Au NPs in PEDOT; therefore no noticeable change is found for PEDOT film properties after incorporation of Au NPs.

Figure 2a shows the dark current density *versus* voltage (*J*−*V*) curve of the tandem solar cell with and

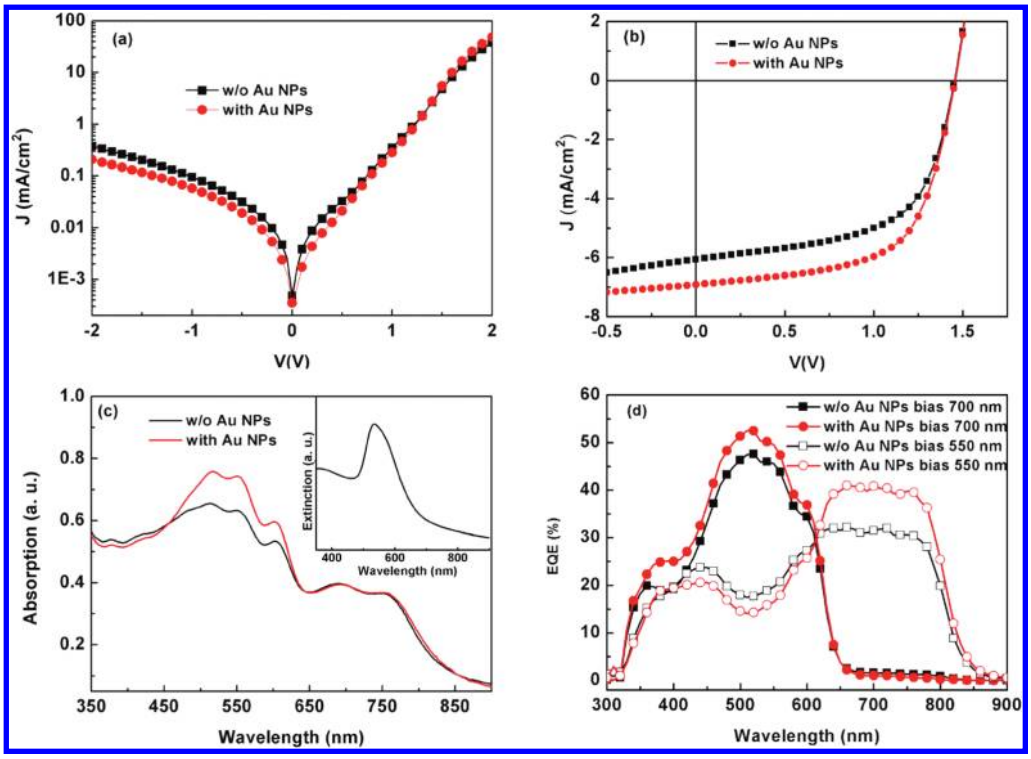

Figure 2. Comparison of tandem cell results with and without Au NPs in the PEDOT:PSS layer: (a) $J-V$ characteristics (dark) of the tandem solar cell, (b) the $J-V$ characteristics of the tandem solar cells under AM1.5G 100 mW·cm^{-2} illumination, (c) absorption of the tandem solar cell, (inset) extinction spectrum of Au solution, and (d) EQE of the tandem solar cell.

without Au NPs. The tandem solar cell shows obvious diode properties, in which at the forward bias the dark current remains in the same order, inferring the series resistance of the multilayer structure has not been reduced by introducing Au NPs into the PEDOT. This is consistent with the conductivity measurement results attained from PEDOT and PEDOT:Au films (see Table S1). To illustrate the effect of the Au NPs on the performance of the tandem solar cell, the $J-V$ characteristics of the proposed tandem solar cell were taken under AM1.5G 100 mW/cm^2 illumination, as shown in Figure 2b, and photovoltaic parameters are listed in Table 1. As shown from the result, after incorporating Au NPs into the PEDOT layer, the open-circuit voltage (V_{OC}) stayed the same, the fill factor (FF) slightly increased from 59.22% to 61.91%, and the short-circuit current (J_{SC}) increased significantly from 6.06 mA/cm^2 to 6.92 mA/cm^2, in which the enhancement ratio was as much as 15%. Consequently, the PCE was improved from 5.22% to 6.24%, in which about 20% enhancement was mainly ascribed to the contribution of the J_{SC} improvement. It is also worth pointing out that the ICL can be fabricated by either spin coating or spray coating, and the corresponding device performances are comparable. To our knowledge, this is the first time obvious J_{SC} and PCE enhancement in a tandem polymer solar cell incorporating a metal particle interlayer has been observed. Previous work on small-molecule organic tandem solar cells showed that inserting a small-size silver cluster between the subcells has two major functions: (1) serving as recombination centers for unpaired charges that are photogenerated in the device's interior[29] and (2) inducing a strong near-field to enhance the absorption of the active layer.[17] In our tandem cell structures, PEDOT and TiO_2:Cs ICL both have good conductivity and can act as good recombination centers for the charge transferred between front and rear cells.[26] In addition, the conductivity of PEDOT with Au NPs is not enhanced, and we can expect no new recombination centers to be introduced after blending Au NPs into the PEDOT layer. This also helps confirming the observation of the FF of tandem cells not being changed significantly with or without Au NPs. In fact, if a 0.5 nm Au thin film was inserted between PEDOT and TiO_2:Cs by thermal evaporation, the J_{SC} and FF of the device stayed at similar values (results are not

TABLE 1. Tandem and Single-Cell Performance with and without Au NPs

device	V_{OC} (V)	J_{SC} (mA/cm^2)	FF (%)	PCE (%)
w/o Au (tandem)	1.455	6.06	59.22	5.22
with Au (tandem)	1.457	6.92	61.91	6.24
w/o Au (front cell)	0.830	6.81	61.81	3.49
with Au (front cell)	0.829	7.95	64.52	4.25
w/o Au (rear cell)	0.630	11.54	39.82	2.89
with Au (rear cell)	0.635	12.65	40.01	3.21

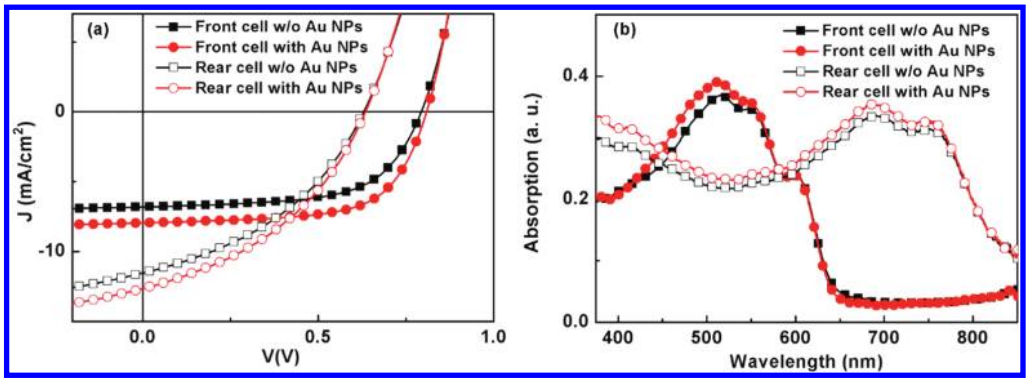

Figure 3. Comparison of single-cell results with and without Au NPs in the PEDOT:PSS layer: (a) current density *versus* voltage ($J-V$) characteristics of the front (ITO/TiO_2:Cs/P3HT:$IC_{60}BA$/PEDOT:PSS/Al) and rear (ITO/PEDOT:PSS/TiO_2:Cs/PSBTBT:$PC_{70}BM$/MoO_3/Al) single cells under AM1.5G 100 mW·cm^{-2} illumination; (b) absorption of front and rear single cells.

shown here). On the basis of these results, it is reasonable to conclude that the enhancement of the current density is mostly due to the absorption improvement from the plasmonic effects of the Au NPs.

To further illustrate the J_{SC} improvement resulting from absorption enhancement, the absorption of tandem solar cells with and without Au NPs was measured, and corresponding results are shown in Figure 2c. The absorption in the region 450 to 650 nm is enhanced significantly after incorporating Au nanoparticles blended into the PEDOT layer, and the region of absorption enhancement is consistent with the measured plasmon resonance region of Au nanoparticles (Figure 2c inset). The insignificant extinction difference between PEDOT and PEDOT:Au (Figure S2) indicated that the absorption enhancement is not related to the absorption of Au NPs. Therefore, we propose that the performance improvement, especially the J_{SC} enhancement of the tandem solar cell, is mainly due to the plasmonic effect of Au NPs, which we can describe as near-field enhancement or light scattering.[19,20] Moreover, we can also see a little enhancement from 750 to 850 nm, which is far from the plasmonic resonance position of the Au NPs. This can be explained by the extension of plasmonic resonance due to Au NP aggregation in the PEDOT layer, as shown in Figure.1d. The external quantum efficiency (EQE) measurements for each subcell of the tandem solar cell were performed. We employed monochromatic light to selectively turn on one of the subcells as photoconductor to conduct accurate EQE measurements for the other subcell,[25,30] for which the results are shown in Figure 2d. It is found that EQEs for both subcells are increased after blending the Au NPs into the PEDOT. Specifically, for the front cell, the maximum EQE increased from 48.1% to 53.1%, and for the rear cell, the maximum EQE increased from 32.6% to 41.7%. It was also found that the EQE of the rear cell with Au NPs decreased by a small amount compared with the reference cell in the region of 400 to 600 nm, explaining that the front cell with Au NPs has fully absorbed the incident light in this region. From these results, we can deduce that the ICL layer with Au NPs enhances both the top and bottom subcells' absorption and EQE simultaneously. By comparing the absorption from Figure 2c with EQE spectra to Figure 2d, we can see that the EQE enhancement is almost coincident with the absorption. Therefore, it is safely concluded that the absorption enhancement is the main reason for EQE enhancement, as well as for PCE enhancement.

To investigate the effect of the PEDOT:Au layer on the tandem solar cell systematically, we studied both the front and rear subcells with and without Au NPs and with the following structures: ITO/TiO_2:Cs/P3HT:$IC_{60}BA$/PEDOT/Al and ITO/PEDOT/TiO_2:Cs/PSBTBT:$PC_{70}BM$/MoO_3/Al. The $J-V$ curve of the front cell with and without Au NPs under AM1.5G 100mW/cm^2 illumination is shown in Figure 3a. Obviously, the short current J_{SC} increased significantly from 6.81 mA/cm^2 to 7.95 mA/cm^2 and FF slightly increased from 61.81% to 64.52%; correspondingly the PCE increased from 3.49% to 4.25%. In order to show the effect of Au NPs on the performance of the rear cell, an additional PEDOT layer was introduced into the rear cell. The $J-V$ curves of the structures are also shown in Figure 3a. Similar to the front cell, the J_{SC} increased from 11.54 to 12.56 mA/cm^2, and V_{OC} and FF stayed the same when Au NPs were blended into the PEDOT. To compare the performance of the single cell with and without Au NPs, the performance parameters of a single cell with and without Au NPs is summarized in Table 1. The absorption spectra of both front and rear cells with and without Au NPs are measured, and the results are shown in Figure 3b. Obviously, the absorption of single cells is enhanced below 650 nm significantly, whereas the absorption of front cells was suppressed beyond 650 nm, leading to only a little enhancement of absorption above 650 nm for the tandem solar cell. The reason for absorption suppression above 650 nm for the front cell is not clear at present. The EQEs of the front and rear cell are both enhanced compared to the device without Au NPs, and the results are shown in

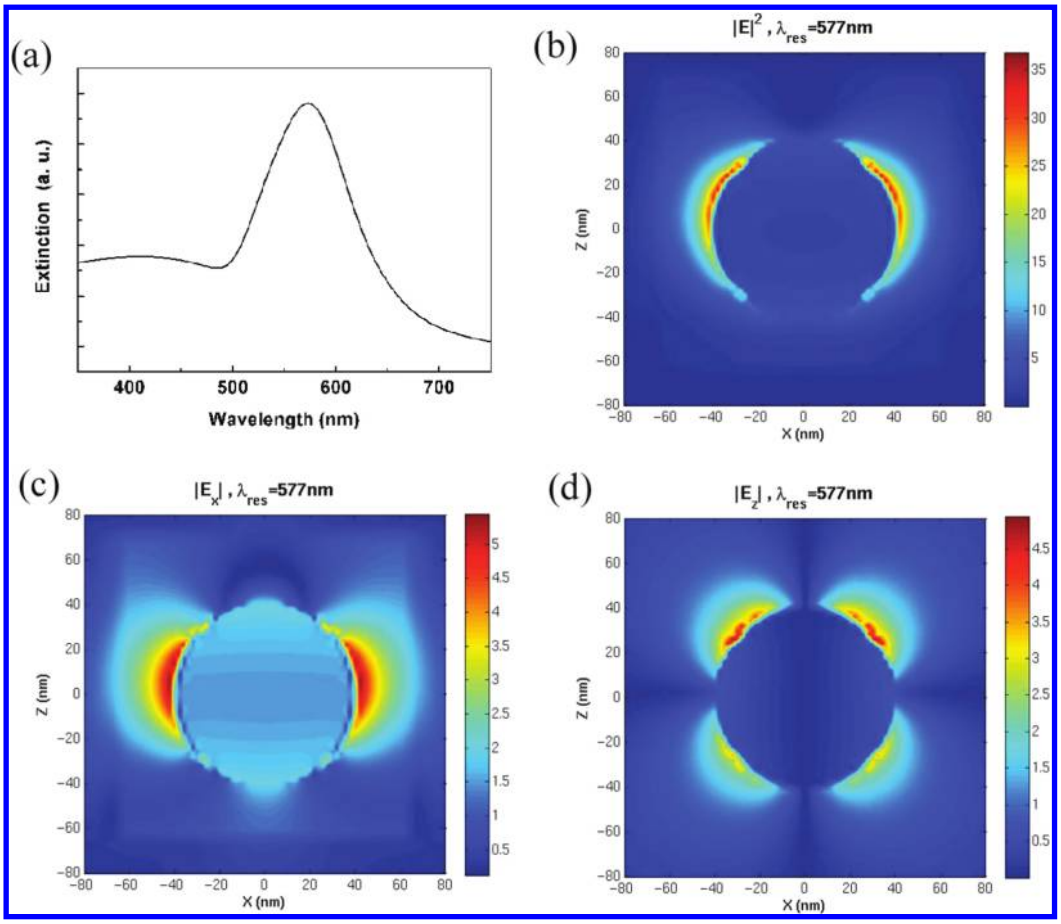

Figure 4. (a) Simulated extinction spectra of isolated Au NPs in PEDOT:PSS (for simplicity, Au NPs are assumed to be isolated from each other); simulated light intensity and electric field distribution around Au NPs at the plasmon resonance position of 577 nm. (b) Light intensity ($|E|^2$) distribution around Au NPs compared with incident light intensity ($|E_0|^2$). (c and d) Electric field distribution along the horizontal (E_x) and vertical (E_z) direction around Au NPs compared with incident light electric field (E_0), respectively.

Figure S3. The EQE enhancement ratio for the rear cell is however not comparable with the absorption enhancement and not well consistent with the *J*−*V* curve. The reason may be the degradation of the device after encapsulation. Above all, the J_{SC} values of the front and rear cells are both increased when introducing Au NPs into the devices, owning to the fact that absorption has been enhanced significantly in the wavelength region from 350 to 700 nm. Simultaneously, the EQE shows the same trend of improvement as the absorption, which indicates that the J_{SC} enhancement could be ascribed to the absorption enhancement *via* plasmonic effects.

Plasmonic-mediated absorption enhancement may be originated from two sources, *i.e.* scattering effect[12] and near-field enhancement effect.[15−17,31,32] In our structures, low-density Au NPs are dispersed in a PEDOT:PSS solution according to Figure S2. The extinction behavior cannot be detected in the resolution. Therefore, the scattering effect from Au NPs can be neglected safely, and it is reasonable to believe that the absorption enhancement coming from the near-field enhancement can be described entirely as a plasmonic effect of the Au nanoparticles. To show the near-field distribution of Au NPs, we assume that the 80 nm size Au NPs are highly dispersed in the PEDOT environment and the particles are isolated from one other (although the Au NPs tend to aggregate in PEDOT from the TEM image shown in Figure 1d; for simplicity in simulation, we still assume the Au NPs are isolated from each other). The simulated extinction cross-section spectra of Au NPs in PEDOT are shown in Figure 4a. As we can see, the resonance position located at 577 nm is red-shift compared with the Au NPs dispersed in water (see the inset of Figure 2c); this difference is ascribed to the different dielectric constant between PEDOT and water. The near-field distribution of Au NPs in PEDOT at resonance wavelength (λ_{res} = 577 nm) is simulated. In our structure, we consider *z* as the polymer growth direction and the light incident direction, *x* is the polarization direction, and the incident light E_0 is normalized. As shown from Figure 4b, it is anticipated that the $|E|^2$ (light intensity, *E* is the electric field) around the Au NPs is enhanced as high as 35-fold compared with the incident light. Clearly, the light has been concentrated by the plasmon of the Au NPs, and

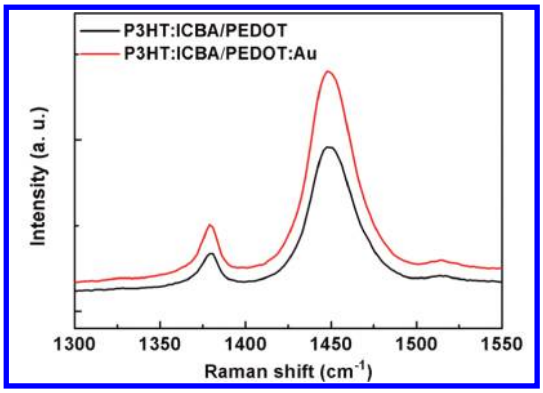

Figure 5. Raman spectra of P3HT:$IC_{60}BA$ capped by a PEDOT:PSS layer with and without Au NPs excited by the Ar^+ laser with a wavelength of 514.5 nm. Raman enhancement due to the plasmonic effect is clearly visible.

thus the absorption of medium around the Au NPs is enhanced, as demonstrated in our experiment. Since plasmon coupling takes place only in its near-field region, the electric fields aligned in the *x* and *z* direction are simulated, and the results are shown in Figure 4c and d, respectively. It is found that the electric field is enhanced in both the *x* and *z* directions in our conditions, and the thickness of PEDOT is about 80 nm, which is very close to the Au NPs' size (70−80 nm). In such a case we can consider that only a single layer of Au NPs is dispersed in the PEDOT and the gap between the front cell and the Au NPs is negligible; therefore the active layers of the front cell can fall in the near-field region of the Au NPs. As for the rear cell, in between PEDOT and the active layer, there is the existence of 10 nm thick TiO_2:Cs as the electron transport layer. As shown in Figure 4d, the active layer of rear cell can still fall in the local near-field of Au NPs, meaning it is also capable of enhancing the rear cell absorption by the near-field of the surface plasmon. In our simulations, we consider only a completely isolated single Au NP. In fact, as shown in Figure 1d, the Au NPs are arranged in a more compact method in the thin film. This will lead to a "hot spot" due to plasmon−plasmon interaction,[33,34] and a much stronger near-field formed by interactions can be expected to result in the attainment of larger absorption enhancement.

To illustrate the strong near-field induced by Au nanoparticles experimentally, we measured the Raman scattering of the P3HT:$IC_{60}BA$ active layer capped by PEDOT with and without Au NPs, and their Raman scattering spectra are shown in Figure 5. The two structures both show an obvious Raman scattering peak at 1448 cm^{-1}, which corresponds to the C═C stretching mode of P3HT.[35] In addition, it also can be found that the P3HT capped by PEDOT with Au NPs has a stronger Raman scattering than the one without Au NPs. As we known, Raman scattering intensity is proportional to the electric field intensity,[36] in which stronger Raman scattering attained from the structure indicates a stronger electric field induced by introducing Au NPs around the active layer. In our Raman scattering measurement, the excitation laser wavelength is 514.5 nm, which is very close to the plasmon resonance position of Au NPs (532 nm for pure Au and 577 nm for PEDOT:Au blend). When the laser is illuminating the Au NPs, a strong local electric field is induced by surface plasmon resonance and Raman scattering is enhanced for the active layer capped Au NPs.[36] These results indicated that a strong near-field is actually induced when introducing Au NPs, which is consistent with the simulated results shown in Figure 4b−d. Theoretical and experimental results both show that a strong near-field is induced around the active layer; therefore, the absorption of the active layer is enhanced by merit of the strong local near-field induced by the metal nanoparticles, and the efficiencies of the front cell, rear cell, and the tandem solar cell are improved accordingly.

CONCLUSION

In conclusion, we have successfully demonstrated a highly efficient plasmonic polymer tandem solar cell by simply incorporating Au NPs into PEDOT:PSS as an ICL. The plasmonic effect happening in the middle of the ICL can potentially enhance both the top and bottom subcells simultaneously, leading to an improvement in the efficiency of the tandem solar cell from 5.22% to 6.24%. The enhancement ratio is as high as 20%. Experimental and theoretical results showed that the enhancement effect was attained from local near-field enhancement of the Au NPs. These results have shown that the plasmonic effect has great potential in the application of polymer solar cells. The proposed interlayer structures as an open platform can be applied to various polymer materials and open up opportunities for highly efficient, multistacked tandem solar cells.

METHODS

Device Fabrication. The device architecture of the plasmonic tandem solar cell is shown in Figure 1a. The tandem cells were fabricated on ITO-coated glass substrates, with a sheet resistance of 15 Ω/□. The precleaned ITO substrates were treated with UV-ozone. The P3HT:$IC_{60}BA$ at a 1:1 weight ratio in 1% DCB solution was spin-casted at 700 rpm for 40 s on top of a layer of TiO_2:Cs. The films were annealed at 150 °C for 5 min. The PEDOT:Au mixture (v/v, 9:1) was spin coated on the first active layer and annealed at 150 °C for 5 min. The Au NPs (0.01% in DI water) with a size of 80 nm were purchased from Nanocs (USA). Then, a thin layer of TiO_2:Cs film was spin-casted, followed by thermal annealing at 150 °C for 10 min. After PSBTBT:$PC_{70}BM$ (1:1) from 1.8% CB solution was spin-casted at 4500 rpm, another thermal

annealing step was performed at 140 °C for 5 min. The device fabrication was completed by thermal evaporation of 15 nm MoO_3 and 100 nm Al as the cathode under vacuum at a base pressure of 2×10^{-6} Torr. For comparison, the device without Au nanoparticles was also fabricated. For TEM measurement, the Au NPs and PEDOT:Au solution were dipped onto the copper grid and dried for measurement, and the measurement was carried out on a JEM 1200-EX (JEOL) .

Electrical, Optical, and Microscopic Characterization of Photovoltaic Cells and Thin Films. *J*−*V* characteristics of photovoltaic cells were taken using a Keithley 4200 source unit under a simulated AM1.5G spectrum with an Oriel 9600 solar simulator. Absorption spectra were taken using a Varian Cary 50 ultraviolet−visible spectrophotometer. Raman scattering was carried out by a Renishawinviaraman microscope. An Ar^+ laser with a wavelength of 514.5 nm was used as an excitation source, and excitation power was 1.25 mW (5% of full power, 25 mW). AFM images were taken on a Digital Instruments multimode scanning probe microscope. To measure EQE of individual subcells in the tandem structure, monochromatic light at 550 and 700 nm was used to excite the bottom (P3HT) and top (PSBTBT) subcells, respectively.

Theoretical Calculation. The extinction spectrum and near-field distribution of Au NPs in PEDOT were simulated by finite difference time domain (FDTD) from Lumerical. The mesh size was 2 nm, and the simulated area was $1 \times 1\ \mu m^2$. For the extinction spectrum, the wavelength region was selected from 350 to 700 nm, and 300 points were chosen. All the dielectric constants are taken from the material database of the software. The dielectric functions of gold and PEDOT:PSS were fitted by the FDTD model to obtain a better simulation.

Acknowledgment. The authors would like to thank Dr. Seiichiro Murase for helping with the TEM and AFM measurements, Dr. Youjun He for supplying $IC_{60}BA$ acceptor, Dr. Rui Zhu and Mr. Yang Yang for supplying TiO_2:Cs solutions, and Mr. Samuel Duan for fruitful discussions. This work was financially supported by the ONR (Grant No. N000141110250), National Science Foundation (Grant No. CHE0822573), and NSFC (Grant No. 50633050 and No. 20821120293).

Supporting Information Available: PEDOT:PSS layer depth profile is shown in Figure S1, absorption of PEDOT and PEDOT:Au film on glass substrate is given in Figure S2, EQE of front and rear single cell with and without Au NPs is shown in Figure S3, and thickness and conductivity of PEDOT:PSS with and without Au NPs are summarized in Table S1. This material is available free of charge *via* the Internet at http://pubs.acs.org.

REFERENCES AND NOTES

1. Coakley, K. M.; McGehee, M. D. Conjugated Polymer Photovoltaic Cells. *Chem. Mater.* **2004**, *16*, 4533–4542.
2. Brabec, C. J.; Sariciftci, N. S.; Hummelen, J. C. Plastic Solar Cells. *Adv. Funct. Mater.* **2001**, *11*, 15–26.
3. Li, G.; Shrotriya, V.; Huang, J.; Yao, Y.; Moriarty, T.; Emery, K.; Yang, Y. High-Efficiency Solution Processable Polymer Photovoltaic Cells by Self-Organization of Polymer Blends. *Nat. Mater.* **2005**, *4*, 864–868.
4. Chen, H. Y.; Hou, J. H.; Zhang, S. Q.; Liang, Y. Y.; Yang, G. W.; Yang, Y.; Yu, L. P.; Wu, Y; Li, G. Polymer Solar Cells with Enhanced Open-Circuit Voltage and Efficiency. *Nat. Photonics* **2009**, *3*, 649–653.
5. Liang, Y. Y.; Xu, Z.; Xia, J. B.; Tsai, S. T.; Wu, Y.; Li, G.; Ray, C.; Lu, L. P. For the Bright Future-Bulk Heterojunction Polymer Solar Cells with Power Conversion Efficiency of 7.4%. *Adv. Mater.* **2010**, *22*, E135–E138.
6. Tvingstedt, K.; Persson, N. K.; Inganas, O.; Rahachou, A.; Zozoulenko, I. V. Surface Plasmon Increase Absorption in Polymer Photovoltaic Cells. *Appl. Phys. Lett.* **2007**, *91*, 113514.
7. Beck, F. J.; Polman, A.; Catchpo, K. R. Tunable Light Trapping for Solar Cells Using Localized Surface Plasmons. *J. Appl. Phys.* **2009**, *105*, 114310.
8. Ferry, V. E.; Sweatlock, L. A.; Pacifici, D.; Atwater, H. A. Plasmonic Nanostructure Design for Efficient Light Coupling into Solar Cells. *Nano Lett.* **2008**, *8*, 4391–4397.
9. Sundararajan, S. P; Grady, N. K.; Mirin, N.; Halas, N. J. Nanoparticle-Induced Enhancement and Suppression of Photocurrent in a Silicon Photodiode. *Nano Lett.* **2008**, *8*, 624–630.
10. Pala, R. A.; White, J.; Barnard, E.; Liu, J.; Brongersma, M. L. Design of Plasmonic Thin-Film Solar Cells with Broadband Absorption Enhancements. *Adv. Mater.* **2009**, *21*, 3504–3509.
11. Hagglund, C.; Apell, S. P.; Kasemo, B. Maximized Optical Absorption in Ultrathin Films and Its Application to Plasmon-Based Two-Dimensional Photovoltaics. *Nano Lett.* **2010**, *10*, 3135–3141.
12. Schaadt, D. M.; Feng, B.; Yu, E. T. Enhanced Semiconductor Optical Absorption *via* Surface Plasmon Excitation in Metal Nanoparticles. *Appl. Phys. Lett.* **2005**, *86*, 063106.
13. Pillai, S.; Catchpole, K. R.; Trupke, T.; Green, M. A. Surface Plasmon Enhanced Silicon Solar Cells. *J. Appl. Phys.* **2007**, *101*, 093105.
14. Kulkarni, A. P.; Noone, K. M.; Munechika, K.; Guyer, S. R.; Ginger, D. S. Plasmon-Enhanced Charge Carrier Generation in Organic Photovoltaic Films Using Silver Nanoprisms. *Nano Lett.* **2010**, *10*, 1501–1505.
15. Morfa, A. J.; Rowlen, K. L.; Reilly, T. H.; Romero, M. J.; Van de Lagemaat, J. Plasmon-Enhanced Solar Energy Conversion in Organic Bulk Heterojunction Photovoltaics. *Appl. Phys. Lett.* **2008**, *92*, 013504.
16. Kim, S. S.; Na, S. I.; Jo, J.; Kim, D. Y.; Nah, Y. C. Plasmon Enhanced Performance of Organic Solar Cells Using Electrodeposited Ag Nanoparticles. *Appl. Phys. Lett.* **2008**, *93*, 073307.
17. Rand, B. P.; Peumans, P.; Forrest, S. R. Long-Range Absorption Enhancement in Organic Tandem Thin-Film Solar Cells Containing Silver Nanoclusters. *J. Appl. Phys.* **2004**, *96*, 7519–7526.
18. Kang, M. G.; Xu, T.; Park, H. J.; Luo, X.; Guo, L. J. Efficiency Enhancement of Organic Solar Cells Using Transparent Plasmonic Ag Nanowire Electrodes. *Adv. Mater.* **2010**, *22*, 4378–4383.
19. Atwater, H. A.; Polman, A. Plasmonics for Improved Photovoltaic Devices. *Nat. Mater.* **2010**, *9*, 205–213.
20. Schuller, J. A.; Barnard, E. S.; Cai, W. S.; Jun, Y. C.; White, J. S.; Brongersma, M. L. Plasmonics for Extreme Light Concentration and Manipulation. *Nat. Mater.* **2010**, *9*, 193–204.
21. Kim, J. Y.; Lee, K.; Coates, N. E.; Moses, D.; Nguyen, T. Q; Dante, M.; Heeger, A. J. Efficient Tandem Polymer Solar Cells Fabricated by All-Solution Processing. *Science* **2007**, *317*, 222–225.
22. Sista, S.; Park, M. H.; Hong, Z. R.; Wu, Y.; Hou, J. H.; Kwan, W. L.; Li, G.; Yang, Y. Highly Efficient Tandem Polymer Photovoltaic Cells. *Adv. Mater.* **2010**, *22*, 380–383.
23. Chen, F. C.; Wu, J. L.; Lee, C. L.; Hong, Y.; Kuo, C. H.; Huang, M. H. Plasmonic-Enhanced Polymer Photovoltaic Devices Incorporating Solution-Processable Metal Nanoparticles. *Appl. Phys. Lett.* **2009**, *95*, 013305.
24. He, Y. J.; Chen, H. Y.; Hou, J. H.; Li, Y. F. Indene-C_{60} Bisadduct: A New Acceptor for High-Performance Polymer Solar Cells. *J. Am. Chem. Soc.* **2010**, *132*, 1377–1382.
25. Chou, C. H.; Kwan, W. L.; Hong, Z. R.; Chen, L. M.; Yang, Y. Metal-Oxide Interconnection Layer for Polymer Tandem Solar Cells with an Inverted Architecture. *Adv. Mater.* **2011**, *23*, 1282–1286.
26. Yang, J.; Zhu, R.; Hong, Z. R.; He, Y. J.; Kumar, A.; Li, Y. F.; Yang, Y. A Robust Inter-Connecting Layer for Achieving High Performance Tandem Polymer Solar Cells. *Adv. Mater.* **2011**, published online, DOI: 10.1002/adma.201100221.
27. Hutter, E.; Fendler, J. H. Exploitation of Localized Surface Plasmon Resonance. *Adv. Mater.* **2004**, *16*, 1685–1706.
28. Lakowicz, J. R. Radiative Decay Engineering 5: Metal-Enhanced Fluorescence and Plasmon Emission. *Anal. Biochem.* **2005**, *337*, 171–194.
29. Yakimov, A; Forrest, S. R. High Photovoltage Multiple-Heterojunction Organic Solar Cells Incorporating Interfacial Metallic Nanoclusters. *Appl. Phys. Lett.* **2002**, *80*, 1667–1669.

30. Gilot, J.; Wienk, M. M.; Janssen, R. A. J. Measuring the External Quantum Efficiency of Two-Terminal Polymer Tandem Solar Cells. *Adv. Funct. Mater.* **2010**, *20*, 3904–3911.
31. Wu, J. L.; Chen, F. C.; Hsiao, Y. S.; Chien, F. C.; Chen, P. L.; Kuo, C. H.; Huang, M. H.; Hsu, C. S. Surface Plasmonic Effects of Metallic Nanoparticles on the Performance of Polymer Bulk Heterojunction Solar Cells. *ACS Nano* **2011**, *5*, 959–967.
32. Diukman, I.; Tzabari, L.; Berkovitch, N; Tessler, N.; Orenstein, M. Controlling Absorption Enhancement in Organic Photovoltaic Cells by Patterning Au Nano Disks within the Active Layer. *Optics Express* **2011**, *19*, A64–A71.
33. Kinkhabwala, A.; Yu, Z. F; Fan, S. H.; Avlasevich, Y.; Mullen, K.; Moerner, W. E. Large Single-Molecule Fluorescence Enhancements Produced by a Bowtie Manoantenna. *Nat. Photonics* **2009**, *3*, 654–657.
34. Ward, D. R.; Pauly, F.; Carlos Cuevas, J.; Natelson, D. Optical Rectification and Field Enhancement in a Plasmonic Nanogap. *Nat. Nanotechnol.* **2010**, *5*, 732–736.
35. Campoy-Quiles, M.; Ferenczi, T.; Agostinelli, T.; Etchegoin, P. G.; Kim, Y.; Anthopoulos, T. D.; Stavrinou, P. N.; Bradley, D. C.; Nelson, J. Morphology Evolution *via* Self-Organization and Lateral and Vertical Diffusion in Polymer:Fullerene Solar Cell Blends. *Nat. Mater.* **2008**, *7*, 158–164.
36. Willets, K. A.; Van Duyne, R. P. Localized Surface Plasmon Resonance Spectroscopy and Sensing. *Annu. Rev. Phys. Chem.* **2007**, *58*, 267–297.